

Published in final edited form as:

Nat Chem. 2021 March 01; 13(3): 243–248. doi:10.1038/s41557-020-00595-w.

## Isolation and electronic structures of derivatized manganocene, ferrocene and cobaltocene anions

Conrad A. P. Goodwin<sup>1,2</sup>, Marcus J. Giansiracusa<sup>1</sup>, Samuel M. Greer<sup>2,3,4</sup>, Hannah M. Nicholas<sup>1</sup>, Peter Evans<sup>1</sup>, Michele Vonci<sup>1</sup>, Stephen Hill<sup>3,5</sup>, Nicholas F. Chilton<sup>1,\*</sup>, David P. Mills<sup>1,\*</sup>

<sup>1</sup>Department of Chemistry, School of Natural Sciences, The University of Manchester, Oxford Road, Manchester, M13 9PL, UK

<sup>2</sup>Chemistry Division, Los Alamos National Laboratory, Los Alamos, NM 87545, USA

<sup>3</sup>National High Magnetic Field Laboratory, Florida State University, Tallahassee, FL 32310, USA

<sup>4</sup>Department of Chemistry & Biochemistry, Florida State University, Tallahassee, FL 32306, USA

<sup>5</sup>Department of Physics, Florida State University, Tallahassee, FL 32306, USA

### Abstract

The discovery of ferrocene nearly 70 years ago marked the genesis of metallocene chemistry; although the ferrocenium cation was discovered soon afterwards, a derivatized ferrocenium dication was only isolated in 2016 and the monoanion of ferrocene has only been observed in low temperature electrochemical studies. Here we report the isolation of a derivatized ferrocene anion in the solid state as part of an isostructural family of 3d metallocenates which consist of anionic complexes of a metal centre (manganese, iron or cobalt) sandwiched between two bulky Cp<sup>ttt</sup> ligands (where Cp<sup>ttt</sup> is {1,2,4-C<sub>5</sub>H<sub>2</sub> tBu<sub>3</sub>}). These air- and thermally-sensitive complexes rapidly decompose above -30 °C, however, we were able to characterise all metallocenates by a wide range of physical techniques and *ab initio* calculations. These data have allowed us to map the electronic structures of this metallocenate family, including an unexpected high-spin  $S = 3/2$  ground state for the 19e<sup>-</sup> derivatized ferrocene anion.

---

The iconic organometallic complex ferrocene, [Cp<sub>2</sub>Fe] (FcH, Cp = cyclopentadienyl, η<sup>5</sup>-C<sub>5</sub>H<sub>5</sub>), was first reported in 1951<sup>1,2</sup>, and the ferrocenium cation [Cp<sub>2</sub>Fe]<sup>+</sup> (FcH<sup>+</sup>) was isolated soon after.<sup>3</sup> These discoveries were the harbingers of metallocene chemistry, which rapidly

---

Users may view, print, copy, and download text and data-mine the content in such documents, for the purposes of academic research, subject always to the full Conditions of use: [http://www.nature.com/authors/editorial\\_policies/license.html#terms](http://www.nature.com/authors/editorial_policies/license.html#terms)

\*Correspondence to: nicholas.chilton@manchester.ac.uk; david.mills@manchester.ac.uk.

#### Author contributions

C. A. P. G. and D. P. M. provided the original concept. C. A. P. G. synthesised and characterised the compounds. H. M. N. and P. E. carried out supporting synthetic and characterisation work. D. P. M. supervised the synthetic component. M. J. G., M. V. and N. F. C. collected and interpreted EPR data. M. V. and N. F. C. performed CASSCF calculations. N. F. C. supervised the EPR and CASSCF components. S. M. G. collected and interpreted Mössbauer spectra, and performed DFT calculations. S. H. supervised S. M. G. and provided additional EPR/Mössbauer interpretation. D. P. M. and N. F. C. wrote the manuscript, with contributions from all authors.

#### Competing interests

The authors declare no competing interests.

spread to cover most of the Periodic Table<sup>4,5</sup>. In the interim ferrocene has become a versatile workhorse in nanotechnology<sup>6</sup>, electrochemistry, catalysis, medicine, and functional materials<sup>7</sup>; industrial applications include fuel additives and the synthesis of agrochemicals and pharmaceuticals<sup>8</sup>. A defining feature of ferrocene is its facile oxidation to ferrocenium, with the fully reversible  $\text{FcH}^{+/0}$  redox couple a standard reference in non-aqueous electrochemical processes<sup>9</sup>.

Whilst metallocenes are strictly defined as the homoleptic  $[\text{Cp}_2\text{M}]$  family, Cp derivatization to  $\text{Cp}^{\text{R}}$  ligands ( $\text{C}_5\text{R}_n\text{H}_{5-n}^-$ ) provides tuneable physicochemical properties<sup>4,5</sup>; for example, decamethylferrocene,  $[\text{Cp}^*\text{Fe}]$  ( $\text{Cp}^* = \text{C}_5\text{Me}_5$ ), can be doubly oxidized to yield dicationic  $[\text{Cp}^*\text{Fe}]^{2+}$  salts<sup>10</sup>. Isolated metallocene anions are conspicuous by their absence in the literature, with “[ $\text{Cp}_2\text{M}$ ]” ( $\text{M} = \text{V}^{11}, \text{Cr}^{11}, \text{Fe}^{12,13}, \text{Co}^{14,15}, \text{Ni}^{11}$ ) and “[ $\text{Cp}_2\text{M}$ ]” ( $\text{M} = \text{Co}, \text{Ni}$ )<sup>15</sup> anions only identified as transient species in seminal low temperature solution-phase electrochemical studies. Notable synthetic results include the reduction of  $[\text{Cp}^*\text{Mn}]$  to an orange powder formulated as “ $\text{Na}[\text{Cp}^*\text{Mn}]$ ”<sup>16,17</sup>, the preparation of white powders of “ $\text{A}[\text{Cp}_2\text{Re}]$ ” ( $\text{A} = \text{Li}^{18}, \text{K}^{19}$ ) from  $[\text{Cp}_2\text{ReH}]$  and  $^n\text{BuLi}$  or  $\text{PhCH}_2\text{K}$ , and the structural characterization of a derivatized *bis*(indenyl) Co anion,  $[\text{Na}(\text{THF})_6][\text{Co}\{\text{C}_9\text{H}_5\text{-1,3-(SiMe}_3)_2\}_2]$ <sup>20</sup>. Recently, potassium salts of  $[\text{Cp}^*\text{Mn}]^-$  were structurally authenticated<sup>21</sup>. It was previously shown that replacement of a  $\text{Cp}^{\text{R}}$  ligand with an arene ( $\text{C}_6\text{R}_6$ ) can provide neutral  $19e^-$  mixed sandwich Fe complexes; some of the  $[(\text{Cp}^{\text{R}})\text{Fe}(\text{C}_6\text{Me}_6)]$  family are stable at room temperature, allowing characterization by single crystal XRD<sup>22,23</sup>. Finally, the related  $19e^-$  Fe *bis*-stannole complex  $[\text{Li}(\text{THF})_4][\text{Fe}\{\text{SnC}_4(\text{SiMe}_3)_2\text{-1,3-Me}_2\text{-2,4}\}_2]$  was recently isolated and structurally authenticated<sup>24</sup>.

Here we report the isolation of an isostructural series of derivatized metallocene anions for Mn, Fe and Co; despite their facile thermal decomposition above  $-30^\circ\text{C}$  these complexes were characterised by a wide range of physical techniques. Together with *ab initio* calculations these studies provide new insights into the electronic structures of metallocenes, including a  $19e^-$  Fe metallocene anion with a high-spin  $S = 3/2$  ground state rather than the low-spin  $S = 1/2$  ground state observed in formally isoelectronic cobaltocenes<sup>4,5</sup>.

## Results and Discussion

### Electrochemistry

We targeted  $[(\text{Cp}^{\text{ttt}})_2\text{M}]^-$  ( $\text{Cp}^{\text{ttt}} = \{1,2,4\text{-C}_5\text{H}_2\text{-}^t\text{Bu}_3\}$ ) anions as the six bulky aliphatic  $^t\text{Bu}$  substituents impart solubility and kinetic stability.  $[(\text{Cp}^{\text{ttt}})_2\text{M}]$  precursors are known for  $\text{M} = \text{Mn}$  (**1**),<sup>25,26</sup>  $\text{Fe}$  (**2**)<sup>27</sup> and  $\text{Co}$  (**3**);<sup>28,29</sup> here we prepared **3** from  $\text{CoCl}_2$  and two equivalents of  $\text{KCp}^{\text{ttt}}$ <sup>30</sup>. We performed cyclic voltammetry on DME solutions of **1-3** at  $-50^\circ\text{C}$  with  $[\text{N}^n\text{Bu}_4][\text{BF}_4]$  as the supporting electrolyte to determine reduction potentials and to assess metallocenate stabilities (Fig. 1). The *quasi*-reversible reduction processes ( $E_{\text{ox/red}}$  (mV) = 760, **1**; 390, **2**; 270, **3**) are similar for **2** and **3**, whilst **1** shows evidence of reactivity on the experimental timescale at negative potentials ( $E_{1/2}$  (V) vs  $\text{FcH}^{+/0} = -3.39$ , **2**;  $-2.49$ , **3**; for **1**  $E_{\text{p1}} = -3.26$  V,  $E_{\text{p2}} = -2.50$  V at peak current density). These reduction waves are all irreversible above  $-30^\circ\text{C}$ , and are formally assigned as  $\text{M}^{2+}/\text{M}^{1+}$  processes from their similarity with the respective voltammograms of  $[\text{Cp}_2\text{M}]$  ( $\text{M} = \text{Fe}$ ,  $-3.45$  to  $-3.57$  V;  $\text{Co}$ ,  $-2.40$  to  $-2.55$  V;

vsFcH<sup>+0</sup>)<sup>12–15</sup> and [Cp\*<sub>2</sub>Mn] (-2.68 V; vsFcH<sup>+0</sup>)<sup>16</sup>; note that for **1** we cannot definitively assign if E<sub>p1</sub> and E<sub>p2</sub> belong to the same redox couple.

## Synthesis

Given the large negative reduction potentials and temperature sensitivity seen in electrochemical studies, we reasoned that low temperature alkali metal reductions would be required to isolate 3d metallocenes; such conditions previously opened up elusive formal +2 oxidation states for f-element Cp<sup>R</sup> complexes<sup>31</sup>. Thus potassium graphite (KC<sub>8</sub>) reductions of **1–3** in THF at -40 °C, in the presence of 2.2.2-cryptand to sequester potassium cations, gave the substituted metallocenes, [K(2.2.2-cryptand)][(Cp<sup>ttt</sup>)<sub>2</sub>M] (M = Mn, **4**; Fe, **5**; Co, **6**) (Fig. 2). Complex **4** reproducibly co-crystallized with one equivalent of [K(2.2.2-cryptand)][Cp<sup>ttt</sup>], thus is formally **4·K(2.2.2-cryptand)Cp<sup>ttt</sup>**; an analogous contaminant [K(2.2.2-crypt)]<sub>2</sub>[(Cp<sup>ttt</sup>)<sub>2</sub>Co][Cp<sup>ttt</sup>] (**7**) was sometimes observed in batches of **6**. The formulations of **4–6** were consistent with values obtained from elemental microanalysis, indicating that the single crystal XRD data is representative of the bulk samples. Intensely coloured THF or DME solutions of **4** (orange), **5** (brown) and **6** (brown) at room temperature change colour within 10 minutes and crystals of **1–3** were isolated from the resultant mixtures, thus all analytical data for **4–6** were collected below -30 °C. Surprisingly the 18e<sup>-</sup> complex **4** is the most thermally sensitive of the series; this is in stark contrast to the derivatized manganocene anion [Cp\*<sub>2</sub>Mn]<sup>-</sup>, which has recently been synthesized by refluxing [Cp\*<sub>2</sub>Mn] with molten K in THF<sup>21</sup>. This temperature sensitivity precluded the collection of reliable magnetic and NMR spectroscopic data for **4–6** despite multiple attempts, but otherwise we were able to fully characterise this family.

## Structural characterisation

The solid-state structures of **1–7** and [K(2.2.2-crypt)][Cp<sup>ttt</sup>] (**8**) were determined by single crystal X-ray diffraction at 150 K. As the [(Cp<sup>ttt</sup>)<sub>2</sub>M] fragments are structurally analogous only the structure of **5** is depicted in Fig. 2 and selected bond lengths and angles are compiled in Table 1; the structures of **1–3** have been reported previously<sup>25–27,29</sup>. In common with **1–3**<sup>25–27,29</sup>, near-eclipsed conformations of the C<sub>5</sub> rings are observed for **4–7**, with the quaternary carbons of <sup>t</sup>Bu groups displaced from the Cp<sup>ttt</sup> C<sub>5</sub> planes away from the metal due to steric crowding. This also causes all the Cp<sup>ttt</sup><sub>centroid</sub>⋯M⋯Cp<sup>ttt</sup><sub>centroid</sub> angles to deviate from linearity, with **5** exhibiting the most bent geometry at 169.38(11)°; in contrast to **4–6**, [K(18-crown-6)(THF)<sub>2</sub>][Cp\*<sub>2</sub>Mn] exhibits a highly axial geometry (Cp\*<sub>centroid</sub>⋯Mn⋯Cp\*<sub>centroid</sub>: 179.5(2)°)<sup>21</sup>. The M–C<sub>Cp</sub> and M⋯Cp<sup>ttt</sup><sub>centroid</sub> distances for **1–7** approximately correlate with valence electron counts, with the shortest values seen for 18e<sup>-</sup> **2** and **4**, and longer distances for 19e<sup>-</sup> **3** and **5**, and 20e<sup>-</sup> **6** and **7**, presumably due to the partial occupancy of antibonding orbitals. As expected, these bond distances increase upon reduction of **2** to **5** and from **3** to **6** or **7**. The seemingly anomalous long distances for 17e<sup>-</sup> **1** are due to its high-spin configuration, which results in significant electron density in antibonding orbitals<sup>26</sup>. The mean Mn⋯Cp<sup>ttt</sup><sub>centroid</sub> distances for **4** (1.750(3) Å) are longer than the corresponding distances in [K(18-crown-6)(THF)<sub>2</sub>][Cp\*<sub>2</sub>Mn] (mean M⋯Cp\*<sub>centroid</sub>: 1.673(7) Å)<sup>21</sup>, due to the greater steric bulk of Cp<sup>ttt</sup> vs Cp\*<sub>2</sub>. 19e<sup>-</sup> **5** exhibits

longer  $M \cdots Cp^{ttt}_{\text{centroid}}$  distances than seen for  $19e^-$  **3**, and  $20e^-$  **6** and **7**, motivating us to analyse their electronic structures.

### Ab initio electronic structure

Given that  $[Cp_2Mn]$  is high-spin<sup>32,33</sup>, but becomes low-spin below 100 K when doped into a diamagnetic matrix of  $[Cp_2Fe]$ <sup>34</sup>, and that  $[Cp^*_2Mn]$  is low-spin<sup>16</sup>, it is evident that electron-electron repulsion and crystal field effects in 3d metallocenes have similar energy scales; indeed, at room temperature 1,1'-dimethylmanganocene shows evidence of both a sextet and doublet ground state<sup>35</sup>. A multiconfigurational wavefunction-based method accounting for electron correlation is therefore the only reliable way of treating the electronic structure, so we performed state-average complete active space self-consistent field (SA-CASSCF) calculations with spin-orbit coupling (SOC) included *a posteriori*, as embodied by the OpenMOLCAS code<sup>36</sup>. For **2-7** the active space consisted of 12 orbitals ( $3d_{xz}$  and  $3d_{yz}$  ( $\pi$ ,  $e_{1g}$ ),  $3d_{z^2}$  ( $\sigma$ ,  $a_{1g}$ ),  $3d_{xy}$  and  $3d_{x^2-y^2}$  ( $\delta$ ,  $e_{2g}$ ), and  $3d_{xz}$  and  $3d_{yz}$  ( $\pi^*$ ,  $e_{1g}$ ) and ligand-hybridised 4d/5d orbitals), while for **1** this active space was not stable and our calculations only included five orbitals ( $3d_{z^2}$  ( $\sigma$ ,  $a_{1g}$ ),  $3d_{xy}$  and  $3d_{x^2-y^2}$  ( $\delta$ ,  $e_{2g}$ ), and  $3d_{xz}$  and  $3d_{yz}$  ( $\pi^*$ ,  $e_{1g}$ )). Here we focus on the metallocenates **4-7**; see Supporting Information for discussion of **1-3**.

For **4**, using an active space of 10 electrons in 12 orbitals (CAS(10,12)+SO, Supplementary Table 13), the ground state is low-spin  $S = 0$  ( $^1A$ ), with a first excited  $S = 1$  state lying at *ca.* 15,000  $cm^{-1}$ . Thus, these calculations suggest that **4** is low-spin diamagnetic just like its isoelectronic partner **2**. For **5**, using CAS(11,12)+SO (Supplementary Table 15) the ground state was found to be high-spin  $S = 3/2$  ( $^4E$ ), but due to the low-symmetry of the molecule the orbital degeneracy of  $3d_{xy}$  and  $3d_{x^2-y^2}$  pair is partly lifted, thus the  $^4E$  is split into two  $S = 3/2$  states separated by *ca.* 1,100  $cm^{-1}$  (subsequent excited states *ca.* 10,000  $cm^{-1}$ ). The ground  $S = 3/2$  state has very large zero-field splitting that can be parameterised by  $D = -36.4$   $cm^{-1}$  and  $|E| = 0.15$   $cm^{-1}$ , meaning that the lowest lying Kramers doublet is  $m_S = \pm 3/2$ , with the  $m_S \pm 1/2$  doublet lying at 72.8  $cm^{-1}$ . The  $g$ -value for the ground state is also anisotropic with  $g_x = g_y = 2.02$ ,  $g_z = 2.72$ , leading to effective  $g$ -values for the ground Kramers doublet of  $g_x = g_y = 0.02$ ,  $g_z = 8.11$ , while those for the first excited doublet are  $g_x = g_y = 4.02(3)$ ,  $g_z = 2.82$ ; the magnetic  $z$ -axis is parallel to the  $Cp^{ttt}_{\text{centroid}} \cdots Fe \cdots Cp^{ttt}_{\text{centroid}}$  vector. Thus, **5** is rather different to its isoelectronic partner **3** which is  $S = 1/2$  ( $^2E$ ). Finally, for the Co metallocenate there are two crystal structures so calculations were performed on both; the first values are for **6** and those in braces are for **7**. Using a CAS(12,12)+SO calculation (Supplementary Tables 17 and 18) the ground state was found to be high-spin  $S = 1$  ( $^3A$ ), with a set of four excited  $S = 1$  states lying between 11,000 – 12,000  $cm^{-1}$  {12,000 – 13,000  $cm^{-1}$ }, and has a sizeable zero-field splitting that can be parameterised by  $D = +25.6$   $cm^{-1}$  and  $|E| = 0.21$   $cm^{-1}$  { $D = +23.6$   $cm^{-1}$  and  $|E| = 0.41$   $cm^{-1}$ }, meaning that the lowest lying state is  $m_S = 0$  with the  $m_S \pm 1$  pseudo-doublet lying at 24 – 26  $cm^{-1}$ , with an intra-doublet separation of 0.4 – 0.8  $cm^{-1}$ . The  $g$ -value for the ground  $S = 1$  state is anisotropic with  $g_x = g_y = 2.17(1)$  and  $g_z = 2.00$  { $g_x = g_y = 2.15(1)$  and  $g_z = 2.00$ }, where the magnetic  $z$ -axis is parallel to the  $Cp^{ttt}_{\text{centroid}} \cdots Co \cdots Cp^{ttt}_{\text{centroid}}$  vector.

## Mössbauer Spectroscopy

Complexes **2** and **5** were studied by  $^{57}\text{Fe}$  Mössbauer spectroscopy (Fig. 3, Supplementary Fig. 68 and Supplementary Table 19). The spectrum of **2** recorded at 80 K consists of a single quadrupole doublet that is best fit with an isomer shift,  $\delta = 0.66(2)$  mm/sec and a quadrupole splitting,  $E_Q = 2.60(2)$  mm/sec (Fig. 3a). The spectrum of **5** displays two quadrupole doublets, unambiguously indicating two Fe species are present in this sample. The first species is described by parameters identical to those of **2**, therefore we assign this doublet to the presence of **2**, which forms upon thermal decomposition of **5** during sample preparation. The second species, which we attribute to **5**, features an asymmetric quadrupole doublet and is fit with  $\delta = 1.25(2)$  mm/sec and  $E_Q = 1.23(2)$  mm/sec (Fig. 3b). The observation of an asymmetric quadrupole doublet is common for Kramers systems, like **5**, in a slow to intermediate relaxation regime, i.e., the relaxation rate is around the same order of magnitude as the  $^{57}\text{Fe}$  Larmor precession (see Supporting Information for further discussion)<sup>37,38</sup>.

The isomer shift quantifies electron density at the  $^{57}\text{Fe}$  nuclei, and hence can be used to identify oxidation state; unfortunately, the isomer shifts in ferrocene ( $\delta \approx 0.45\text{--}0.6$ )<sup>39,40</sup> and associated cations ( $\delta \approx 0.51\text{--}0.62$  for  $1^+$ <sup>41</sup>,  $\delta \approx 0.59$  mm/sec for  $2^+$ <sup>10</sup>) are similar. The isomer shift range of previously reported formally  $\text{Fe}^{1+}$  sandwich complexes ( $\sim 0.52\text{--}0.73$  at 77 K)<sup>23,24,38,42</sup> are smaller than that observed for **5**, but these literature examples almost exclusively exhibit low spin ground states; herein, we propose that **5** has a formal  $4s^0 3d^7$  high spin ground state with a reduced Fe spin population of +2.82 (see below).

To rationalize the unusually large isomer shift we have performed DFT calculations with hybrid (B3LYP) and GGA (BP86) functionals (Supplementary Table 20). The calculated isomer shifts and quadrupole splitting parameters of **2** ( $\delta^{\text{calc}} = 0.61\text{--}0.69$  mm/sec,  $|E_Q^{\text{calc}}| = 2.51\text{--}3.37$  mm/sec) are in excellent agreement with the experimental values ( $\delta = 0.66(2)$  mm/sec,  $|E_Q| = 2.60(2)$  mm/sec). In the case of **5**, the calculated isomer shift for the high ( $\delta^{\text{calc}} = 1.09\text{--}1.27$  mm/sec) and low ( $\delta^{\text{calc}} = 1.14\text{--}1.31$  mm/sec) spin state both agree with the experimental value ( $\delta = 1.25(2)$  mm/sec). Unfortunately, comparison of the calculated quadrupole splitting for the high ( $|E_Q^{\text{calc}}| = 0.65\text{--}0.68$  mm/sec) and low ( $|E_Q^{\text{calc}}| = 2.01\text{--}2.36$  mm/sec) spin states to the experimental one ( $E_Q = 1.23(2)$  mm/sec) is not useful for determination of the spin state.

## EPR Spectroscopy

To directly probe the spin ground states of **1-7** we performed continuous wave EPR spectroscopy at X- (*ca.* 9.4 GHz) and Q-band (*ca.* 34 GHz) on polycrystalline samples. For brevity, we focus here on the data for **3** and **5**, and summarize the results of the remaining compounds while providing a full analysis in the Supporting Information; we note that a continuous wave X-band EPR spectrum of a DCM frozen solution of **3** at 100 K has been reported previously<sup>28</sup>. As expected for the  $18e^-$  ferrocene analogue **2**, there is no EPR spectrum at any temperature at X- or Q-band, in agreement with an  $S = 0$  ground state from CASSCF calculations. Similarly, the  $18e^-$  **4** is also EPR silent at X- and Q-band aside from signals arising from the presence of **1** (Supplementary Fig. 74). The X-band EPR spectrum at 5 K for **3** ( $\text{Co}^{2+}$ ) shows a single feature around  $g = 1.89$  (Supplementary Fig. 72),

suggesting a low-spin  $S = 1/2$  ground state, but a Q-band spectrum at 11 K reveals additional structure (Fig. 4a). Frozen solution experiments confirm an extrinsic peak in the powder spectrum at  $g_{iso} = 1.83$  (Supplementary Fig. 73), and simulations of the solid state data with Easyspin<sup>43</sup> give  $g_x = 2.00$ ,  $g_y = 1.93$  and  $g_z = 1.72$  with hyperfine interaction with the  $^{59}\text{Co}$   $I = 7/2$  nuclear spin  $A_x = 400$ ,  $A_y = 0$  and  $A_z = 150$  MHz (Fig. 4a; we note that these hyperfine coupling constants are approximate due to the unresolved nature of the hyperfine structure).

X-band EPR spectra of **5** between 5 and 20 K show a broad resonance between 0.1 and 0.3 T that increases in intensity with increasing temperature (Supplementary Fig. 75). Only a weak spectrum could be obtained at Q-band (Fig. 4b), which shows a large positive feature at 0.5 T and a smaller negative feature at 1 T, suggestive of an easy-plane-like effective doublet state. Taken together with the temperature dependence of the X-band spectra, these results are consistent with an EPR-active excited state with easy-plane anisotropy. We hypothesise that this signal arises from an  $S = 3/2$  ground state with negative axial zero field splitting (ZFS,  $D < 0$ ) such that the ground  $m_S = \pm 3/2$  Kramers doublet (which would appear as easy-axis) is EPR silent and the excited  $m_S = \pm 1/2$  doublet (which behaves as easy-plane) is EPR active. Fitting the variable temperature X-band and Q-band spectra simultaneously<sup>44</sup> gives  $D = -4.42$  with  $E = 0$  and  $g_{x/y} = 2.06$  and  $g_z = 2.37$  (Fig. 4b and Supplementary Fig. 75), though we note that the magnitude of  $D$  is given solely by the temperature dependence of the X-band spectra, and is thus not spectroscopically determined and should be treated as an estimate.

Resonances in the Q-band EPR spectra of **5** are at different magnetic fields to those seen for **3** (Fig. 4), indicating different effective  $g$ -values, which are far from  $g = 2$  for **5** (effective  $g$ -values are  $g_z = 2.37$  and  $g_{x/y} = 4.12$ ). This provides strong foundation for the assignment of **5** as arising from a  $S = 3/2$  spin state, in addition to the temperature dependence, as the large effective  $g$ -values are very unlikely to arise from a  $S = 1/2$  system. Indeed, Rajasekharan *et al.* show that the  $g$ -values for variously substituted low-spin  $d^7$  mixed sandwich  $[(\eta^5\text{-C}_5\text{R}_5)\text{Fe}(\eta^6\text{-C}_6\text{R}_6)]$  complexes are between 1.2 and 2.1<sup>45</sup>, which are consistent with our EPR data for **3** ( $g_x = 2.00$ ,  $g_y = 1.93$  and  $g_z = 1.72$ ) but clearly distinct from the data for **5** (effective  $g$ -values of  $g_z = 2.37$  and  $g_{x/y} = 4.12$ , arising from  $S = 3/2$ ,  $D = -4.42$   $\text{cm}^{-1}$  with  $E = 0$   $\text{cm}^{-1}$  and  $g_{x/y} = 2.06$  and  $g_z = 2.37$ ). CASSCF-SO calculations agree well with experimental data, predicting an axially anisotropic  $S = 1/2$  ground state for **3** with  $g$ -values of  $g_x \approx g_y = 2.1$ ,  $g_z = 1.61$ , and a ground  $S = 3/2$  spin state with negative uniaxial magnetic anisotropy for **5**, however the experimental  $D$  value for **5** is far smaller than that calculated ( $-4.42$  *cf.*  $-36.4$   $\text{cm}^{-1}$ ). Low  $g$ -values  $< 2$  are unusual for greater-than-half-filled d-shell complexes such as **3** and  $[(\eta^5\text{-C}_5\text{R}_5)\text{Fe}(\eta^6\text{-C}_6\text{R}_6)]$ <sup>45</sup>, and arise from the low-spin configuration where a single unpaired electron resides in a near-degenerate pair of  $\pi^*$  orbitals (Fig. 5) where the orbital doublet degeneracy is lifted by low-symmetry perturbations, which has a parallel to the electronic structure and EPR spectra of  $d^3$   $\text{Fe}^{5+}$  nitrido and oxo complexes<sup>46</sup>. The negative  $D$  value for **5** in the high-spin  $^4\text{E}$  ground state is a result of the uneven occupation of three electrons in the near-degenerate  $d_{xy/x^2-y^2}$  ( $\delta$  symmetry) orbitals (Fig. 5) leading to a significant contribution of orbital angular momentum along the z-direction and domination of the  $D_{zz}$  component of the  $D$ -tensor<sup>47</sup>.



The difference in the ground spin states of **3** and **5** is likely a result of the compressed coordination sphere experienced by the metal in **3**, due to stronger dipolar interactions and shorter bond lengths for  $\text{Co}^{2+}$  (Table 1). This effect is analogous to that of high- and low-spin monomeric manganocenes<sup>26</sup>. Such changes in bonding clearly affect 3d orbital energies, and it is commonplace to see orbital occupation diagrams of metallocenes from theoretical calculations. However, orbital energies are a single electron construct, and thus are non-existent in a wavefunction where electron correlation is explicitly considered. While we cannot produce orbital energy diagrams, we can use the state-averaged occupation of the active orbitals to infer their energetic ordering; that is, orbitals with greater occupation are lower in energy relative to those with lower occupation, Fig. 5. The orbital orderings for **2** and **4** are the same, but differ from the “traditional” picture<sup>48</sup> of  $d_{xz}/d_{yz} (\pi, e_{1g}) < d_{xy}/d_{x^2-y^2} (\delta, e_{2g}) < d_{z^2} (\sigma, a_{1g}) < d_{xz}/d_{yz} (\pi^*, e_{1g})$  (recently echoed by a density-functional theory study<sup>49</sup>) and also from that determined with Hartree-Fock theory of  $d_{z^2} (\sigma, a_{1g}) < d_{xy}/d_{x^2-y^2} (\delta, e_{2g}) < d_{xz}/d_{yz} (\pi, e_{1g}) < d_{xz}/d_{yz} (\pi^*, e_{1g})$ <sup>50</sup>. The orbital orderings for **5-7** are the same as one-another, yet differ from all other orderings already discussed, and are the same as that accepted for the ferrocenium cation<sup>50</sup>. Complex **3** is the clear outlier from our results here, where the  $d_{xz}/d_{yz} (\pi, e_{1g})$  orbitals are the HOMO-1, and this ordering is in agreement with the Hartree-Fock results on ferrocene<sup>50</sup>. All of the occupation numbers (Supplementary Tables 8, 9, 11, 13, 15, 17, 18) suggest that  $d_{z^2} (\sigma, a_{1g})$  lies lower than the  $d_{xy}/d_{x^2-y^2}$  pair ( $\delta, e_{2g}$ ), although for **2-4** and **6-7** the average occupations are quite close (1.97(1) and 1.93(2), respectively) so that these orbitals may be quite close in energy; for **5** there is a much more significant difference in the occupation numbers of 1.96 and 1.48, respectively, clearly indicating that  $d_{z^2}$  is lower in energy than  $d_{xy}/d_{x^2-y^2}$ . The difference between this ordering and that of the “traditional” picture must owe to electron correlation effects, but we re-iterate that orbital energies do not exist in multi-reference wavefunctions such as those calculated here and so these orderings are only indicative.

The synthetic methodology presented herein should be transferable to other d-block metallocenates with appropriate functionalization. We note that these results come over 50 years after the first published efforts to reduce ferrocene with alkali metals<sup>51</sup>. In the first report of the electrochemical reduction of cobaltocene in 1974, Geiger predicted that metallocene anions would be interesting candidates to study electrophilic attack at metallocene centres<sup>14</sup>; such reactivity studies on structurally authenticated ferrocene monoanions are now plausible. We envisage that the isolation of thermally stable examples will facilitate more rapid progress in this endeavour<sup>21</sup>, as well as providing systems that are more amenable to magnetic and spectroscopic characterisation.

## Methods

### General procedures

All manipulations were performed using standard Schlenk techniques or in an Inert Purelab HE 2GB glovebox. Solvents were dried by passing through columns containing activated alumina and molecular sieves, or by refluxing over potassium followed by distillation, and were degassed before use. Complexes were variously characterised by cyclic voltammetry, single crystal X-ray diffraction (a Rigaku XtalLAB AFC11 or Rigaku Oxford Diffraction

SuperNova diffractometer equipped with CCD area detectors), elemental microanalysis, NMR, EPR, FTIR, Raman and UV-Vis-nIR spectroscopies, and DFT and CASSCF calculations; complexes **2** and **5** were additionally studied by  $^{57}\text{Fe}$  Mössbauer spectroscopy.  $[(\text{Cp}^{\text{ttt}})_2\text{M}]$  (**1-3**) were prepared by salt metathesis protocols from the parent  $\text{MCl}_2$  and two equivalents of  $\text{KCp}^{\text{ttt}}$  in THF under reflux conditions, and were isolated by removal of volatiles in vacuo followed by recrystallization from hexane, by adapting published procedures<sup>25-27,29</sup>.  $[\text{K}(2.2.2\text{-crypt})][(\text{Cp}^{\text{ttt}})_2\text{M}]$  (**4-6**) were prepared by reduction of parent **1-3** with  $\text{KC}_8$ <sup>52</sup> in the presence of 2.2.2-cryptand in THF at  $-40\text{ }^\circ\text{C}$ , and were isolated by filtration and layering with hexane at  $-40\text{ }^\circ\text{C}$ . See below for example syntheses of **3** and **5**.

### Synthesis of $[(\text{Cp}^{\text{ttt}})_2\text{Co}]$ (**3**)

THF (20 mL) was added to a pre-cooled ( $-78\text{ }^\circ\text{C}$ ) mixture of  $\text{CoCl}_2$  (0.390 g, 3.0 mmol) and  $\text{KCp}^{\text{ttt}}$  (1.635 g, 6.0 mmol) in a grease-free Teflon stoppered vessel (Rotaflo), then allowed to warm slowly to room temperature. As the mixture warmed the solution slowly turned dark brown. The mixture was heated at  $80\text{ }^\circ\text{C}$  for 16 hrs, which produced dark brown solution with a pale precipitate. The mixture was cooled, and the volatiles were removed *in vacuo* to afford a brown solid. Hexane (30 mL) was added, and the mixture heated at  $80\text{ }^\circ\text{C}$  for 3 hrs, cooled to room temperature, and filtered away from pale solids. The solution was concentrated to  $\sim 1.5\text{ mL}$  and stored at  $5\text{ }^\circ\text{C}$  for 16 hrs, giving **3** ( $\text{C}_6\text{H}_{14}$ ) as large brown plates (1.076 g, 59%). Anal. Calcd (%) for  $\text{C}_{34}\text{H}_{58}\text{Co}\cdot\text{C}_6\text{H}_{14}$ : C, 78.51; H, 11.86. Found: C, 79.36; H, 11.82.  $^1\text{H}$  NMR ( $\text{C}_6\text{D}_6$ , 400 or 500 MHz, 298 K):  $\delta = 3.50$  (br. s), 3.67 (br. s).  $^{13}\text{C}\{^1\text{H}\}$  NMR ( $\text{C}_6\text{D}_6$ , 125 MHz) No peaks were observed. FTIR (ATR, microcrystalline):  $\tilde{\nu} = 402$  (w), 424 (w), 436 (w), 453 (w), 477 (w), 494 (w), 504 (w), 524 (m), 538 (w), 549 (w), 565 (w), 598 (m), 612 (w), 620 (w), 632 (w), 640 (w), 659 (w), 675 (w), 693 (w), 702 (w), 708 (w), 718 (w), 724 (w), 742 (w), 753 (w), 777 (w), 791 (w), 826 (w), 842 (w), 850 (w), 873 (w), 885 (w), 904 (w), 916 (w), 926 (w), 948 (w), 977 (w), 1003 (w), 1016 (w), 1056 (m), 1065 (m), 1073 (m), 1097 (m), 1128 (m), 1152 (w), 1163 (w), 1173 (w), 1201 (m), 1234 (s), 1260 (s), 1275 (m), 1297 (s), 1328 (m), 1354 (vs), 1387 (s), 1409 (m), 1446 (m), 1458 (m), 1477 (s), 1511 (m), 1540 (m), 1575 (m), 1589 (m), 1617 (w), 1634 (w), 1674 (w), 1699 (m), 1732 (w), 1758 (w), 1781 (m), 1819 (m), 1858 (m), 1882 (m), 1891 (m), 1909 (m), 1938 (m), 1962 (m), 1976 (s), 2009 (s), 2033 (m), 2048 (m), 2072 (m), 2131 (w), 2148 (m), 2156 (m), 2254 (m), 3016 (s).  $^1\text{H}$  NMR spectroscopy was in agreement with earlier reports<sup>28,29</sup>.

### Synthesis of $[\text{K}(2.2.2\text{-crypt})][(\text{Cp}^{\text{ttt}})_2\text{Fe}]$ (**5**)

THF (2 mL) was added to a mixture of **2** (0.366 g, 0.7 mmol), and 2.2.2-cryptand (0.264 g, 0.7 mmol) to give a bright ruby-red solution. This solution was added rapidly to a pre-cooled ( $-78\text{ }^\circ\text{C}$ ) Schlenk vessel containing  $\text{KC}_8$  (0.095 g, 0.7 mmol) and a Teflon-coated stirrer bar. The slurry was stirred rapidly and allowed to warm to  $-40\text{ }^\circ\text{C}$  over the course of 10 minutes, during which time the colour changed from ruby-red to dark brown. The mixture was stirred at  $-40\text{ }^\circ\text{C}$  for 10 minutes, and then allowed to settle for a further 5 minutes. The brown solution was filtered cold to a pre-cooled ( $-40\text{ }^\circ\text{C}$ ) vessel, and concentrated at this temperature to *ca.* 1 mL. Hexane (4 mL) was carefully layered on top, which caused some crystals to immediately form. The vessel and cold bath were transferred to a freezer ( $-25\text{ }^\circ\text{C}$ ), to warm slowly to  $-25\text{ }^\circ\text{C}$  overnight. Brown blocks of **5** were isolated by cold filtration



(0.140 g, 21%). Anal. Calcd (%) for  $C_{52}H_{94}O_6N_2KFe$ : C, 66.57; H, 10.10; N, 2.99. Found: C, 66.60; H, 10.47; N, 3.03.  $^1H$  NMR ( $C_4D_8O$ , 400 MHz, 298 K):  $\delta$  = -8.12 (s, 18H, FWHM = 186 Hz,  $C_5H_2(CMe_3)$ ), -2.70 (s, 36H, FWHM = 423 Hz,  $(C_5H_2(CMe_3)_2)$ ), 2.28 – 2.78 (36H, 2.2.2-cryptand),  $Cp^{III}-CH$  not observed.  $^{13}C\{^1H\}$  NMR ( $C_4D_8O$ , 125 MHz) 35.76, 55.45, 57.43, 69.59, 70.51, 71.85, 72.96, 126.19, 127.00. FTIR (ATR, microcrystalline):  $\tilde{\nu}$  = 406 (m), 414 (w), 428 (m), 447 (w), 459 (w), 467 (w), 483 (w), 524 (m), 563 (m), 591 (w), 661 (w), 667 (w), 753 (m), 777 (m), 791 (m), 832 (m), 850 (w), 930 (m), 950 (s), 983 (m), 995 (m), 1026 (m), 1077 (s), 1085 (s), 1103 (vs), 1132 (s), 1195 (w), 1234 (m), 1260 (m), 1275 (w), 1295 (m), 1328 (w), 1352 (m), 1385 (m), 1446 (m), 1458 (m), 1477 (m), 1509 (w), 1542 (w), 1575 (w), 1591 (w), 1630 (w), 1644 (w), 1674 (w), 1699 (w), 1719 (w), 1734 (w), 1754 (w), 1781 (w), 1791 (w), 1821 (w), 1836 (w), 1852 (w), 1878 (w), 1895 (w), 1905 (w), 1915 (w), 1938 (w), 1962 (w), 1978 (w), 2009 (w), 2035 (w), 2046 (w), 2068 (w), 2164 (w), 2168 (w), 2239 (w), 2280 (w), 2317 (m), 2341 (w), 2372 (w), 2815 (m), 2882 (m), 2949 (m), 3018 (w), 3049 (w), 3059 (w), 3067 (w), 3076 (w), 3086 (w), 3096 (w), 3104 (w), 3114 (w), 3123 (w).

## Electrochemistry

All electrochemistry experiments were initially assessed at the open circuit potential and redox potentials are referenced to the  $FcH^{+/0}$  couple (unless otherwise stated) which was used as an internal standard. Cyclic voltammetry was carried out using a sealed cell and a three-electrode arrangement, with a Pt wire working electrode, Pt flag secondary electrode and an  $AgCl/Ag$  wire *pseudo*-reference electrode prepared by soaking a Ag wire in  $FeCl_3(aq)$  before rinsing with water and acetone. Where measurements are performed at low temperature, the cell was equilibrated back to room temperature after each scan and stirred thoroughly before cooling in a  $-50^\circ C$  acetone/liquid nitrogen bath without stirring (at least 1 minute to equilibrate) then transferred back into the Faraday cage and measurements performed promptly to minimize warming.

## CASSCF calculations

OpenMolcas v18.09 was used for all calculations<sup>36</sup>, employing the unoptimized XRD structure of each complex, with counterions and/or solvent removed, and include a sphere of point charges (+2 for  $M^{2+}$ , +1 for  $M^{1+}$ , -0.2 for Cp-ring carbon atoms, +1 for  $K^+$  counterions) of 40 Å radius to model the crystalline electric potential. Basis functions for all atoms are from the ANO-RCC library<sup>53,54</sup>, using VTZP quality for the 3d metal atom, VDZP quality for the 10 Cp-ring carbon atoms, and VDZ quality for all other atoms. We use the second-order DKH transformation for the relativistic Hamiltonian and Cholesky decomposition with a threshold of  $10^{-8}$  for the two-electron integrals. We start with an active space of five 3d orbitals (nominally  $3d_{z^2}$  ( $\sigma$ ,  $a_{1g}$ ),  $3d_{xy}$  and  $3d_{x^2-y^2}$  ( $\delta$ ,  $e_{2g}$ ), and  $3d_{xz}$  and  $3d_{yz}$  ( $\pi^*$ ,  $e_{1g}$ )), and use the RAS probing method<sup>55</sup> to locate two bonding 3d ( $3d_{xz}$  and  $3d_{yz}$  ( $\pi$ ,  $e_{1g}$ )) and five excited 4d orbitals to include them in the active space, and subsequently optimise the orbitals using SA-CASSCF for all states below *ca.* 40,000  $cm^{-1}$  for each spin multiplicity (relative energies). Then, we re-optimize the orbitals by considering only the lowest-lying well-isolated states for each multiplicity. In the last step, we perform a configuration interaction expansion in the optimized active space to find roots that are below 30,000  $cm^{-1}$  for each spin multiplicity (relative energies), and then mix all states with SOC.

## Mössbauer Spectroscopy

Spectra were recorded at 80 K in zero applied field using a constant acceleration spectrometer and a  $^{57}\text{Co}/\text{Rh}$  source. The samples used for these measurements consisted of ground powders of **2** and **5** that were contained in PEEK (polyether ether ketone) sample cups with tightly fitted lids. The isomer shift is reported relative to that of  $\alpha\text{-Fe}$  at room temperature. Spectral simulations were generated using the WMOSS software package (SEE Co. Minneapolis, MN).

## EPR spectroscopy

EPR samples were prepared as ground powders and flame sealed under inert atmosphere while keeping the sample at 77 K in 2 mm Q-band and 4 mm X-band tubes. A frozen solution sample of **3** was prepared at 5 mM concentration in a mixed 9:1 toluene:*n*-hexane solvent system. The solution sample was frozen in liquid nitrogen then loaded into the spectrometer. Spectra were collected using Bruker EMX300 and E500 spectrometers. Low temperature measurements were achieved using liquid helium cooling to obtain 5 K. A strong pitch standard of  $g = 2.0028$  was used to calibrate the magnetic field.

## Supplementary Material

Refer to Web version on PubMed Central for supplementary material.

## Acknowledgements

We acknowledge funding from the Engineering and Physical Sciences Research Council (Doctoral Prize Fellowship to C. A. P. G., EP/N007034/1 for M. V., EP/R002605X/1 for P. E., studentship for H. M. N. and EP/K039547/1 for a single crystal X-ray diffractometer), the Royal Society (University Research Fellowship to N. F. C.), European Research Council CoG-816268 (for D. P. M. and M. J. G.) and StG-851504 (for N. F. C.) and the University of Manchester (Presidential Doctoral Prize to M. J. G.). C. A. P. G. and S. M. G. thank the Laboratory Directed Research and Development (LDRD) program at Los Alamos National Laboratory (an affirmative action/equal opportunity employer, managed by Triad National Security, LLC, for the NNSA of the U. S. Department of Energy (contract 89233218CNA000001) for a distinguished J. Robert Oppenheimer Postdoctoral Fellowship, and Directors Fellowship, respectively. S. H. acknowledges support of the National Science Foundation (DMR-1610226). We thank the EPSRC U. K. National Electron Paramagnetic Resonance Service for access to the EPR Facility and the University of Manchester for access to the Computational Shared Facility. A portion of this work was performed at the National High Magnetic Field Laboratory, which is supported by the National Science Foundation Cooperative Agreement No. DMR-1644779 and the State of Florida. We also thank Fabrizio Ortu for assistance with the collection of Raman spectra. This project has received funding from the European Research Council (ERC) under the European Union's Horizon 2020 research and innovation programme (grant agreement Nos. 816268 and 851504).

## Data availability statement

Supplementary information is available in the online version of the paper. Reprints and permissions information is available online at [www.nature.com/reprints](http://www.nature.com/reprints). Correspondence and requests for materials should be directed to N. F. C. and D. P. M. Crystallographic data for the structures reported in this Article have been deposited at the Cambridge Crystallographic Data Centre, under deposition numbers CCDC 1951767 (**1**), 1951768 (**2**), 1951769 (**3**), 1951770 (**4**), 1951771 (**5**), 1951772 (**6**), 1951773 (**7**) and 1951774 (**8**). Copies of the data can be obtained free of charge from the CCDC via [www.ccdc.cam.ac.uk/structures](http://www.ccdc.cam.ac.uk/structures). Raw research data files supporting this publication are available from Mendeley Data at doi:10.17632/rzpcwgkx5.1. Apart from the data sets mentioned, all other data

supporting the findings of this study are available within the Article and Supplementary information.

## References

1. Kealy TJ, Pauson PL. A New Type of Organo-Iron Compound. *Nature*. 1951; 168:1039–1040.
2. Miller SA, Tebboth JA, Tremaine JF. 114. *Dicyclo* pentadienyliron. *J Chem Soc*. 1952:632–635.
3. Wilkinson G, Rosenblum M, Whiting MC, Woodward RB. THE STRUCTURE OF IRON BIS-CYCLOPENTADIENYL. *J Am Chem Soc*. 1952; 74:2125–2126.
4. Long, NJ. *Metalloenes - An Introduction to Sandwich Complexes*. Blackwell Science; Oxford: 1998.
5. Togni, A, Halterman, RL. *Metalloenes: Synthesis Reactivity Applications*. Wiley-VCH; Weinheim: 1998.
6. Fukino T, et al. Manipulation of Discrete Nanostructures by Selective Modulation of Noncovalent Forces. *Science*. 2014; 344:499–540. [PubMed: 24786075]
7. Astruc D. Why is Ferrocene so Exceptional? *Eur J Inorg Chem*. 2017:6–29.
8. Jumde RP, Lanza F, Veenstra MJ, Harutyunyan SR. Catalytic asymmetric addition of Grignard reagents to alkenyl-substituted aromatic *N*-heterocycles. *Science*. 2016; 352:433–437. [PubMed: 27102477]
9. Connelly NG, Geiger WE Jr. Chemical Redox Agents for Organometallic Chemistry. *Chem Rev*. 1996; 96:877–910. [PubMed: 11848774]
10. Malischewski M, Adelhardt M, Sutter J, Meyer K, Seppelt K. Isolation and structural and electronic characterization of salts of the decamethylferrocene dication. *Science*. 2016; 353:678–682. [PubMed: 27516596]
11. Holloway JDL, Bowden WL, Geiger WE Jr. Unusual electron-transfer processes involving electron-rich and electron-deficient metallocenes. *J Am Chem Soc*. 1997; 99:7089–7090.
12. Mugnier Y, Moise C, Tirouflet J, Laviron E. Reduction electrochimique du ferrocene. *J Organomet Chem*. 1980; 186:C49.
13. Ito N, Saji T, Aoyagui S. Electrochemical formation of stable ferrocene anion and the formal rate constant of the ferrocene<sup>0/-</sup> electrode. *J Organomet Chem*. 1983; 247:301–305.
14. Geiger WE Jr. Electroreduction of cobaltocene. Evidence for a metallocene anion. *J Am Chem Soc*. 1974; 96:2632–2634.
15. Bard AJ, Garcia E, Kukharensko S, Strelets VV. Electrochemistry of metallocenes at very negative and very positive potentials. Electrogeneration of 17-electron Cp<sub>2</sub>Co<sup>2+</sup>, 21-electron Cp<sub>2</sub>Co<sup>2-</sup>, and 22-electron Cp<sub>2</sub>Ni<sup>2-</sup> species. *Inorg Chem*. 1993; 32:3528–3531.
16. Smart JC, Robbins JL. A low spin manganocene and its novel anionic derivative. Synthesis and characterization of decamethylmanganocene complexes. *J Am Chem Soc*. 1978; 100:3936–3937.
17. Robbins JL, Edelstein NM, Cooper SR, Smart JC. Syntheses and electronic structures of decamethylmanganocenes. *J Am Chem Soc*. 1979; 101:3853–3857.
18. Baudry D, Ephritikhine M. Reactions de (η<sup>5</sup>-C<sub>5</sub>H<sub>5</sub>)<sub>2</sub>ReH et de ses derives. preparation de nouveaux complexes biscyclopentadienyles du rhenium. *J Organomet Chem*. 1980; 195:213–222.
19. Gardner BM, McMaster J, Lewis W, Liddle ST. Synthesis and structure of [{N(CH<sub>2</sub>CH<sub>2</sub>NSiMe<sub>3</sub>)<sub>3</sub>}URe(η<sup>5</sup>-C<sub>5</sub>H<sub>5</sub>)<sub>2</sub>]: a heterobimetallic complex with an unsupported uranium-rhenium bond. *Chem Commun*. 2009:2851–2853.
20. Hung-Low F, Bradley CA. Synthesis of a Bis(indenyl) Co(I) Anion: A Reactive Source of a 14 Electron Indenyl Co(I) Equivalent. *Inorg Chem*. 2013; 52:2446–2457. [PubMed: 23427933]
21. Malischewski M, Seppelt K. Structural characterization of potassium salts of the decamethylmanganocene anion Cp\*<sub>2</sub>Mn<sup>-</sup>. *Dalton Trans*. 2019; 48:17078–17082. [PubMed: 31701989]
22. Astruc D, Román EE, Hamon JR, Batail P. Novel reactions of dioxygen in organometallic chemistry. Hydrogen atom abstraction vs. dimerization of the 19-electron complexes η<sup>5</sup>-cyclopentadienyliron(I) η<sup>6</sup>-arene. *J Am Chem Soc*. 1979; 101:2240–2242.

23. Hamon JR, Astruc D, Michaud P. Syntheses, characterizations, and stereoelectronic stabilization of organometallic electron reservoirs: the 19-electron  $d^7$  redox catalysts  $\eta^5\text{-C}_5\text{R}_5\text{Fe-}\eta^6\text{-C}_6\text{R}'_6$ . *J Am Chem Soc.* 1981; 103:758–766.
24. Saito M, Matsunaga N, Hamada J, Furukawa S, Tada T, Herber RH. Anionic Stannaferrocene and Its Unique Electronic State. *Chem Lett.* 2019; 48:163–165.
25. Sitzmann H, Schär M, Dormann E, Kelemen M. High Spin-Manganocenes with Bulky, Alkylated Cyclopentadienyl Ligands. *Z Anorg Allg Chem.* 1997; 623:1609–1613.
26. Walter MD, Sofield CD, Booth CH, Andersen RA. Spin Equilibria in Monomeric Manganocenes: Solid-State Magnetic and EXAFS Studies. *Organometallics.* 2009; 28:2005–2019.
27. Walter MD, White PS.  $[\text{Cp}'\text{Fe}]_2$  as convenient entry into iron-modified pincer complexes: bimetallic  $\eta^6, \kappa^1$ -POCOP-pincer iron iridium compounds. *New J Chem.* 2011; 35:1842–1854.
28. Schneider JJ, et al. Synthesis, structure and spectroelectrochemistry of bis( $\eta^6$ -1,4-tri-*tert*-butylbenzene)chromium(0) and bis( $\eta^5$ -1,2,4-tri-*tert*-butyl-cyclopentadienyl)cobalt(II). Dia- and paramagnetic sandwich complexes derived from sterically highly demanding  $\pi$ -ligands. *J Organomet Chem.* 1999; 590:7–14.
29. Peters M, et al. Pogo-Stick Iron and Cobalt Complexes: Synthesis, Structures, and Magnetic Properties. *Inorg Chem.* 2019; 58:16475–16486. [PubMed: 31769666]
30. Jaroschik F, Nief F, Le Goff X-F, Ricard L. Synthesis and Reactivity of Organometallic Complexes of Divalent Thulium with Cyclopentadienyl and Phospholyl Ligands. *Organometallics.* 2007; 26:3552–3558.
31. Woen, DH, Evans, WJ. Expanding the + 2 Oxidation State of the Rare-Earth Metals, Uranium, and Thorium in Molecular Complexes. *Handbook on the Physics and Chemistry of Rare Earths.* Bünzli, J-CG, Pecharsky, VK, editors. Vol. 50. Elsevier B. V; Amsterdam: 2016. 337–394.
32. Fischer EO, Leipfinger H. Weitere magnetische Untersuchungen zur Struktur der Cyclopentadien- und Inden-Verbindungen der Übergangsmetalle. *Z Naturforsch.* 1955; 10b:353–355.
33. Wilkinson G, Cotton FA, Birmingham JM. On manganese cyclopentadienide and some chemical reactions of neutral *bis*-cyclopentadienyl metal compounds. *J Inorg Nucl Chem.* 1956; 2:95–113.
34. Walter MD, Sofield CD, Andersen RA. Spin equilibria and thermodynamic constants for  $(\text{C}_5\text{H}_4\text{R})_2\text{Mn}$ , R = H or Me in solid solutions of diamagnetic diluents. *J Organomet Chem.* 2015; 776:17–22.
35. Switzer ME, Wang R, Rettig MF, Maki AH. Electronic ground states of manganocene and 1,1'-dimethylmanganocene. *J Am Chem Soc.* 1974; 96:7669–7674.
36. Fdez. Galván I, et al. OpenMolcas: From Source Code to Insight. *J Chem Theory Comput.* 2019; 15:5925–5964. [PubMed: 31509407]
37. Wickman HH, Klein MP, Shirley DA. Paramagnetic Hyperfine Structure and Relaxation Effects in Mossbauer Spectra:  $\text{Fe}^{57}$  in Ferrichrome. *A Phys Rev.* 1966; 152:345.
38. Stoian SA, Yu Y, Smith JM, Holland PL, Bominaar EL, Münck E, Mössbauer, Electron Paramagnetic Resonance, and Crystallographic Characterization of a High-Spin Fe(I) Diketiminato Complex with Orbital Degeneracy. *Inorg Chem.* 2005; 44:4915–4922. [PubMed: 15998018]
39. Wertheim GK, Herber RH.  $\text{Fe}^{57}$  Mössbauer Effect in Ferrocene Derivatives. *J Chem Phys.* 1963; 38:2106–2111.
40. Stukan RA, Gubin SP, Nesmeyanov AN, Gol'danskii VI, Makarov EF. A Mössbauer study of some ferrocene derivatives. *Theor Exper Chem.* 1966; 2:581–584.
41. Reiners M, Baabe D, Schweyen P, Freytag M, Jones PG, Walter MD. Study on Spin-Lattice Relaxation Processes in *tert*-Butyl Substituted Ferrocenium Derivatives. *Eur J Inorg Chem.* 2017:388–400.
42. Mariot JP, Michaud P, Lauer S, Astruc D, Trautwein AX, Varret F. Mössbauer study and molecular orbital calculations on the organo-iron (I, II) electron reservoir sandwiches  $\text{CpFe}^{n+}(\eta^6\text{-C}_6(\text{CH}_3)_6)$  ( $n = 0, 1$ ) and related  $\text{CpFe}(\text{cyclohexadienyl})$  complexes. *J Physique.* 1983; 44:1377–1385.
43. Stoll S, Schweiger A. EasySpin, a comprehensive software package for spectral simulation and analysis in EPR. *J Magn Reson.* 2006; 178:42–55. [PubMed: 16188474]
44. Chilton NF, Anderson RP, Turner LD, Soncini A, Murray KS. PHI: A powerful new program for the analysis of anisotropic monomeric and exchange-coupled polynuclear  $d$ - and  $f$ -block complexes. *J Comput Chem.* 2013; 34:1164–1175. [PubMed: 23386394]

45. Rajasekharan MV, Giezyński S, Ammeter JH, Oswald N, Hamon JR, Astruc D, Michaud P. EPR studies of the electronic structure and dynamic Jahn-Teller effect in iron(I) sandwich compounds. *J Am Chem Soc.* 1982; 104:2400–2407.
46. Chang H-C, et al. Electron Paramagnetic Resonance Signature of Tetragonal Low Spin Iron(V)-Nitrido and -Oxo Complexes Derived from the Electronic Structure Analysis of Heme and Non-Heme Archetypes. *J Am Chem Soc.* 2019; 141:2421–2434. [PubMed: 30620571]
47. Gomez-Coca S, Cremades E, Aliaga-Alcalde N, Ruiz E. Mononuclear Single-Molecule Magnets: Tailoring the Magnetic Anisotropy of First-Row Transition-Metal Complexes. *J Am Chem Soc.* 2013; 135:7010–7018. [PubMed: 23586965]
48. Molloy, KC, editor. Chapter 10 - Ferrocene. *Group Theory for Chemists (Second Edition)*. Woodhead Publishing; 2013. 109–118.
49. Cirera J, Ruiz E. Electronic and Steric Control of the Spin-Crossover Behavior in [(Cp<sup>R</sup>)<sub>2</sub>Mn] Manganocenes. *Inorg Chem.* 2018; 57:702–709. [PubMed: 29283254]
50. Ishimura K, Hada M, Nakatsuji H. Ionized and excited states of ferrocene: Symmetry adapted cluster-configuration-interaction study. *J Chem Phys.* 2002; 117:6533–6537.
51. Watt GW, Baye LJ. Reactions of metallocenes with potassium and potassium amide in liquid ammonia. *J Inorg Nucl Chem.* 1964; 26:2099–2102.
52. Bergbreiter DE, Killough JM. Reactions of potassium-graphite. *J Am Chem Soc.* 1978; 100:2126–2134.
53. Roos BO, Lindh R, Malmqvist P-Å, Veryazov V, Widmark P-O. Main Group Atoms and Dimers Studied with a New Relativistic ANO Basis Set. *J Phys Chem A.* 2004; 108:2851–2858.
54. Roos BO, Lindh R, Malmqvist P-Å, Veryazov V, Widmark P-O. New Relativistic ANO Basis Sets for Transition Metal Atoms. *J Phys Chem A.* 2005; 109:6575–6579. [PubMed: 16834004]
55. Veryazov V, Malmqvist PÅ, Roos BO. How to select active space for multiconfigurational quantum chemistry? *Int J Quant Chem.* 2011; 111:3329–3338.

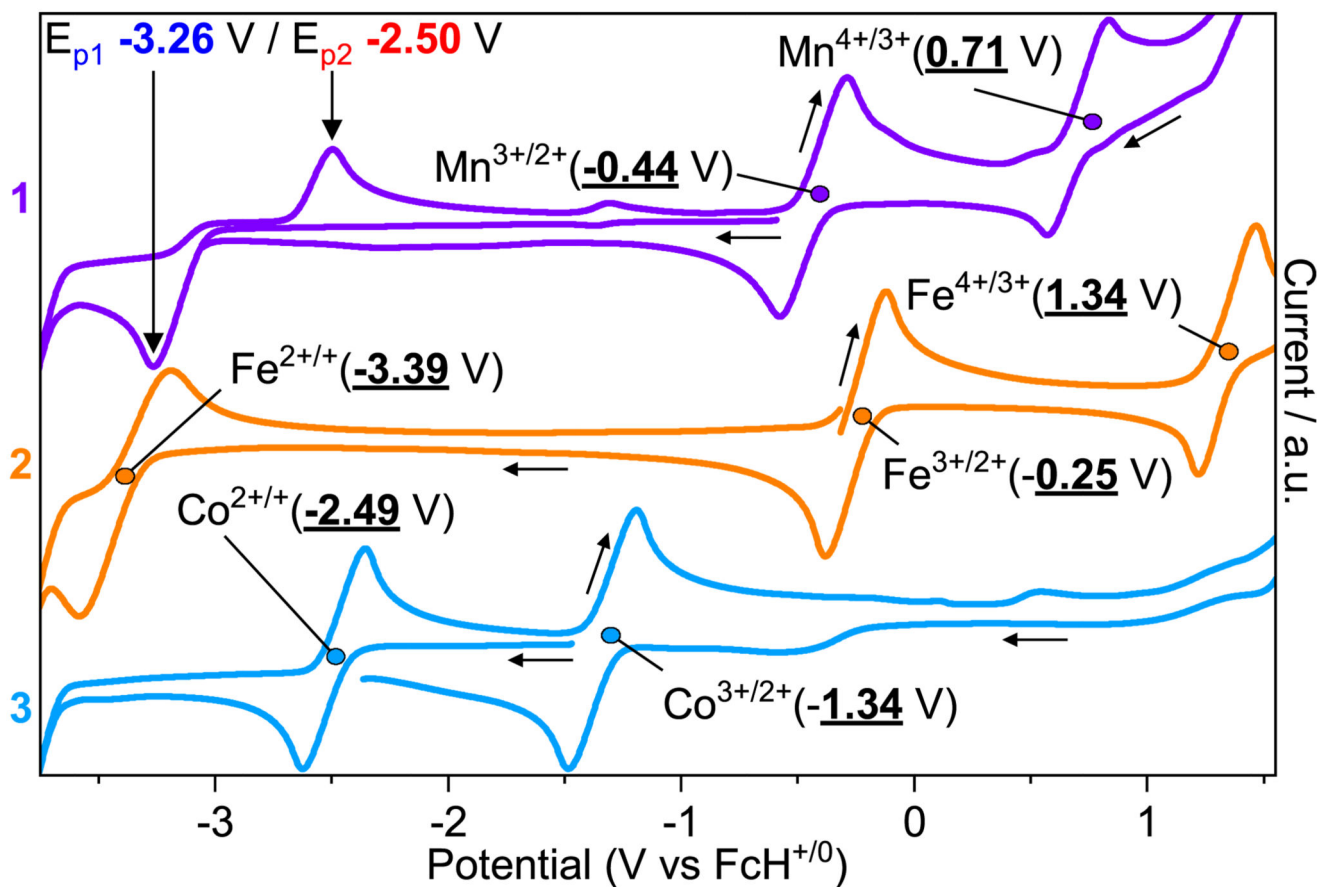


**Figure 1. Electrochemical studies for 1-3.**

Cyclic voltammograms (current in arbitrary units, a.u., vs Potential, V vs FcH<sup>+/0</sup>) of **1** (Mn, purple), **2** (Fe, orange), **3** (Co, blue) at -50 °C, 1 mM in DME with 0.5 M [N<sup>n</sup>Bu<sub>4</sub>][BF<sub>4</sub>] (**1** and **3**, 200 mV/s; **2**, 100 mV/s), with redox processes labelled with formal metal oxidation states and arrows to indicate scan direction. As the formal Mn<sup>2+/+</sup> redox couple of **1** is not reversible, the peak potentials are denoted (E<sub>p1</sub>/E<sub>p2</sub>) at the point of peak current density. The table compiles The table compiles half-wave (E<sub>1/2</sub>) or peak potential values (V vs FcH<sup>+/0</sup>) for the electrochemical redox processes [(Cp<sup>ttt</sup>)<sub>2</sub>M]<sup>0/-</sup>, [(Cp<sup>ttt</sup>)<sub>2</sub>M]<sup>+0</sup>, and [(Cp<sup>ttt</sup>)<sub>2</sub>M]<sup>2+/+</sup> for complexes **1-3** when observed.



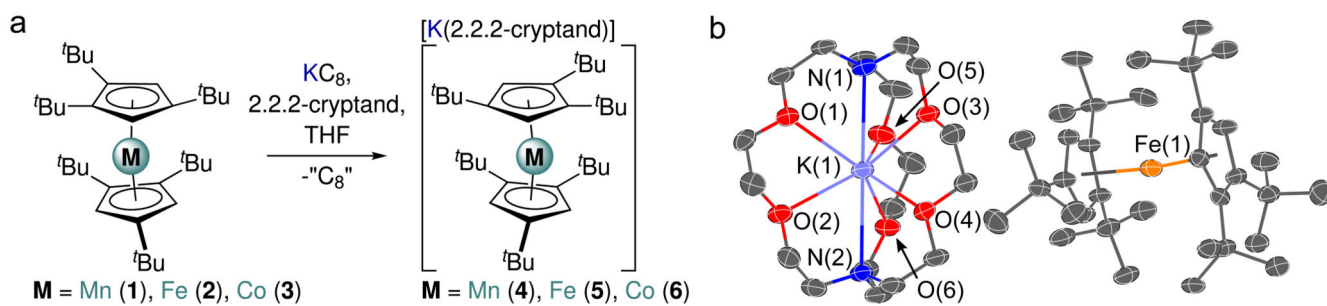
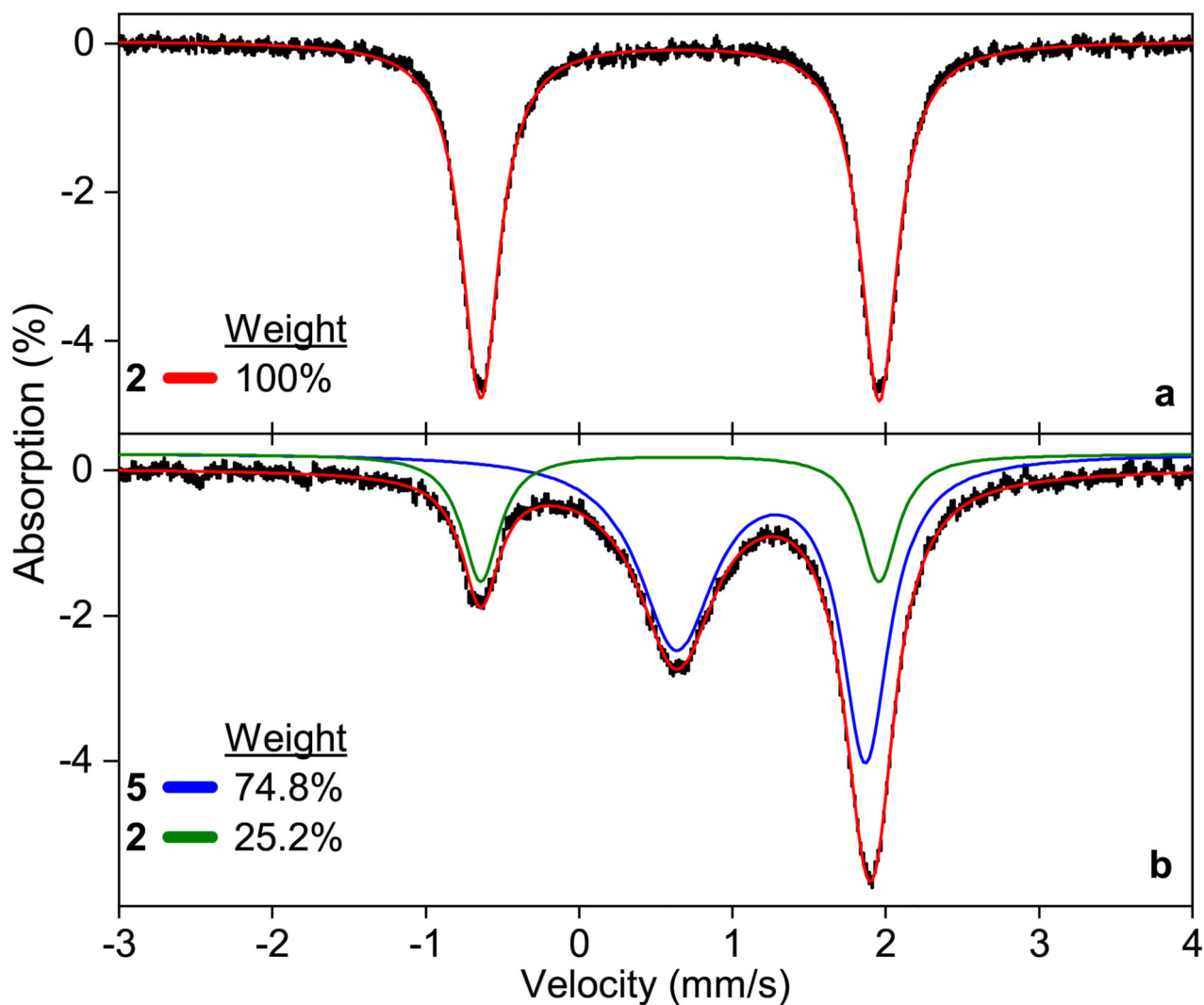


**Figure 2. Synthesis of 4-6 and molecular structure of 5.**

**a**, Synthesis of complexes **4-6**. **b**, Molecular structure of **5** with selective atom labelling (Fe, orange; K, violet; O, red; N, blue; C, grey). Displacement ellipsoids set at 50 % probability level and hydrogen atoms are omitted for clarity.



Sample / Site (mm/s)	$\delta$	$\Delta E_Q$	$\Gamma_L$	$\Gamma_R$
<b>2 / N</b>	0.66(2)	2.60(2)	0.3	0.3
<b>5 / A</b>	1.25(2)	1.23(2)	0.6	0.38
<b>5 / N</b>	0.66(2)	2.60(2)	0.3	0.3

**Figure 3. Zero-field  $^{57}\text{Fe}$  Mössbauer spectra for 2 and 5.**

$^{57}\text{Fe}$  Mössbauer spectra of powders recorded under zero applied magnetic field and 80 K (% Absorption vs Velocity, mm/s): a) Sample of  $[(\text{Cp}^{\text{III}})_2\text{Fe}]$  (**2**); experimental (black) and simulated (red); b) Sample of  $[\text{K}(2.2.2\text{-cryptand})][(\text{Cp}^{\text{III}})_2\text{Fe}]$  (**5**); the blue trace corresponds to the quadrupole doublet assigned to **5** (~75%) whilst the green trace originates from the presence of **2** that forms upon the thermal decomposition of **5** (~25%). The red trace is the weighted sum of the two sub-spectra. The table compiles the experimentally determined  $^{57}\text{Fe}$  Mössbauer parameters for the sites (independent Fe environments) in the two samples **2**

and **5**, with N referring to the parameters of the Neutral molecule  $[(\text{Cp}^{\text{ttt}})_2\text{Fe}]$ , and A to the Anion,  $[(\text{Cp}^{\text{ttt}})_2\text{Fe}]^-$ . The following parameters are shown:  $\delta$ , the isomer shift;  $E_Q$ , the quadrupole splitting;  $\Gamma_L$  and  $\Gamma_R$ , the line widths at half maximum showing the asymmetry of the doublet for **5**. Here, the numbers in parentheses indicate the estimated uncertainty in the last digit.

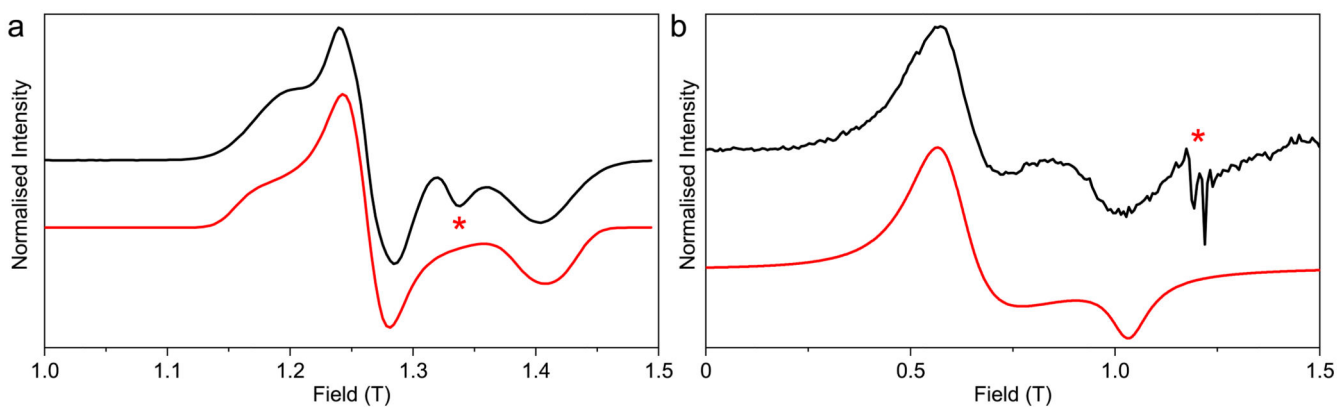


**Figure 4. Continuous wave Q-band EPR spectra of 3 and 5.**

**a, 3** at 11 K (33.950645 GHz, red line is a simulation with  $S = 1/2$ ,  $g_x = 2.00$ ,  $g_y = 1.93$  and  $g_z = 1.72$  with  $A_x = 400$ ,  $A_y = 0$  and  $A_z = 150$  MHz and  $Iw_{iso} = 30$  mT using Easyspin<sup>41</sup>). **b, 5** at 5 K (34.080627 GHz, red line is a simulation with  $S = 3/2$ ,  $D = -4.42$  cm<sup>-1</sup> with  $E = 0$  cm<sup>-1</sup> and  $g_{x/y} = 2.06$  and  $g_z = 2.37$ ,  $Iw_{x/y} = 12.9$  and  $Iw_z = 3.7$  GHz using PHI<sup>42</sup>). Stars denote extrinsic peaks. The resonances observed for **5** are at different magnetic fields to those seen for **3**, and consistent with an assignment of **5** having a  $S = 3/2$  spin state.

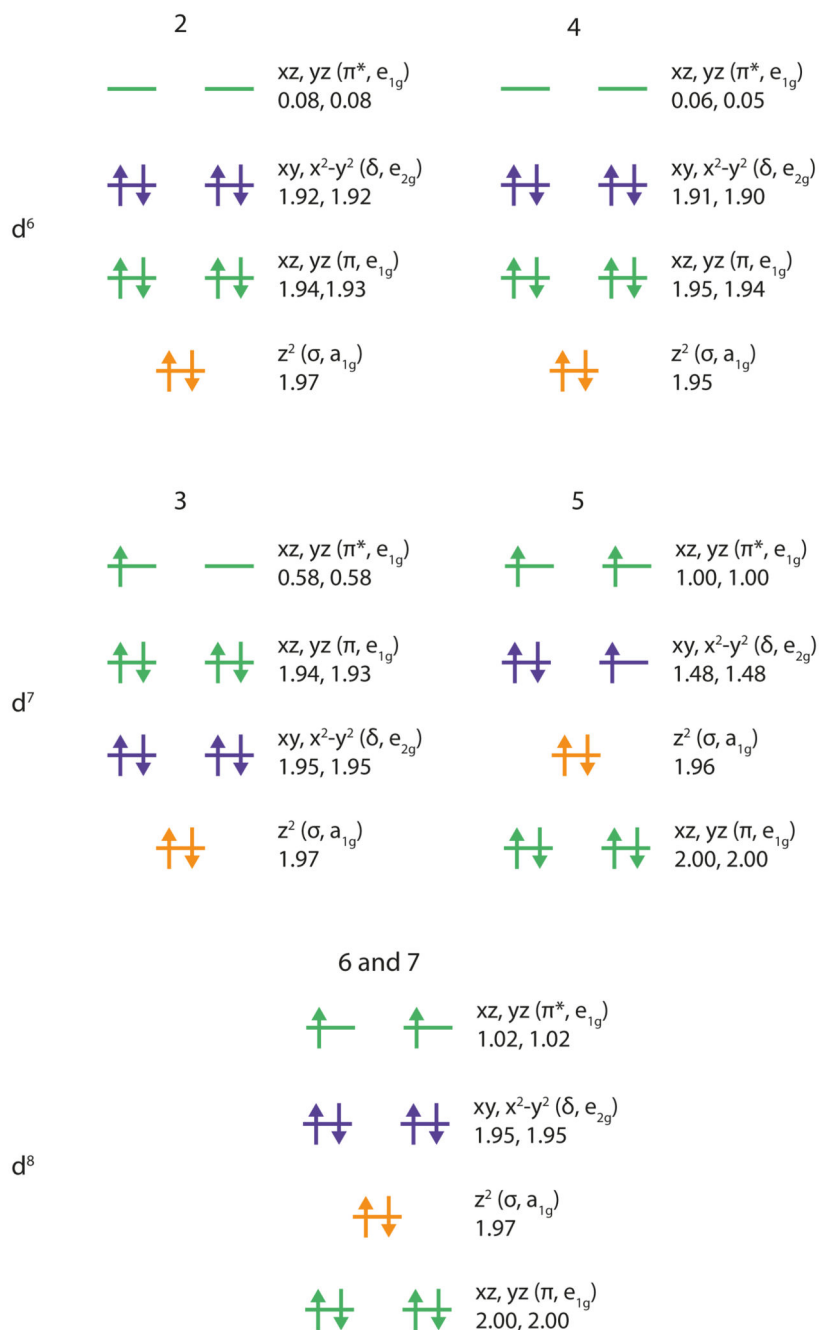


**Figure 5. Orbital ordering, occupation, and approximate symmetry labels for the active space of 2-7 from CASSCF-SO.**

Energy separation is not to scale and is merely indicative, visualised occupations are rounded (the occupations for **6** and **7** are identical, and those shown for **2** are Fe1; those for Fe2 are nearly identical), and the five excited 4d orbitals are excluded. Note that each diagram has four electrons more than the formal  $d^n$  configuration, corresponding to the formally bonding  $\pi, e_{1g}$  electrons.

**Table 1**

Selected distances (Å) and angles (°) for **1-7** (data for **1-3** agree with references 25, 27 and 29).

Complex	Range M–C <sub>p</sub>	Mean M···Cp <sup>ttt</sup> <sub>centroid</sub>	Cp <sup>ttt</sup> <sub>centroid1</sub> ···M···Cp <sup>ttt</sup> <sub>centroid2</sub>	Formal e <sup>-</sup> count
<b>1</b>	2.347(2) – 2.516(2)	2.105(2)	169.63(3)	17
<b>2</b>	2.034(3) – 2.156(3)	1.715(2)	174.91(8)	18
<b>3</b>	2.121(2) – 2.227(2)	1.802(2)	174.77(4)	19
<b>4</b>	2.099(4) – 2.159(4)	1.750(3)	174.68(9)	18
<b>5</b>	2.262(5) – 2.511(6)	2.064(4)	169.38(11)	19
<b>6</b>	2.220(3) – 2.451(3)	1.958(2)	175.96(5)	20
<b>7</b>	2.225(2) – 2.415(2)	1.930(2)	176.20(5)	20